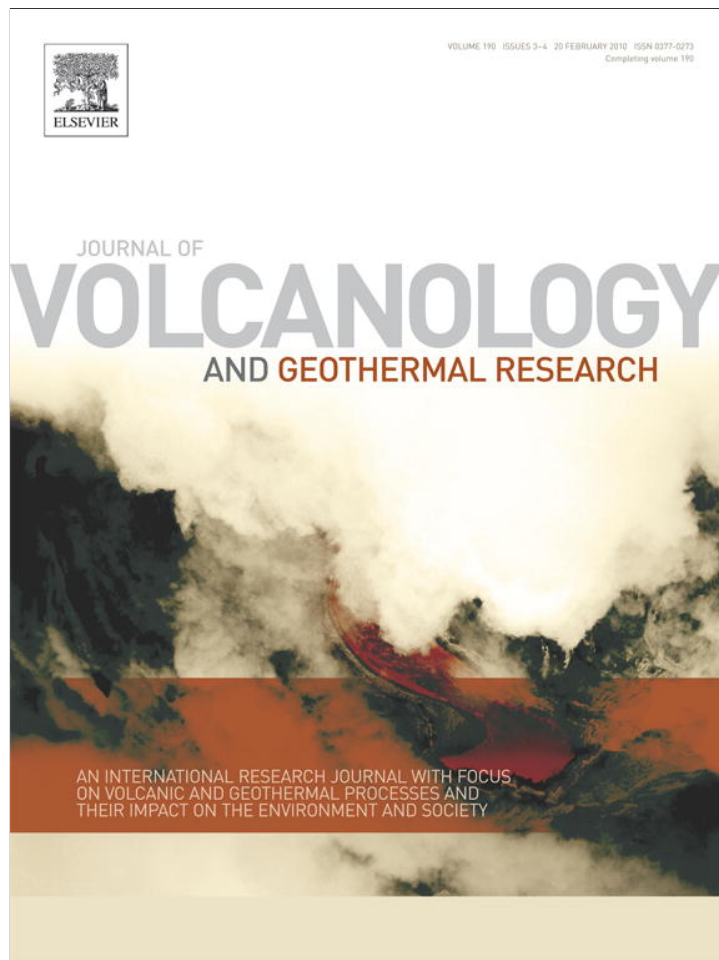


Provided for non-commercial research and education use.
Not for reproduction, distribution or commercial use.



This article appeared in a journal published by Elsevier. The attached copy is furnished to the author for internal non-commercial research and education use, including for instruction at the authors institution and sharing with colleagues.

Other uses, including reproduction and distribution, or selling or licensing copies, or posting to personal, institutional or third party websites are prohibited.

In most cases authors are permitted to post their version of the article (e.g. in Word or Tex form) to their personal website or institutional repository. Authors requiring further information regarding Elsevier's archiving and manuscript policies are encouraged to visit:

<http://www.elsevier.com/copyright>



Contents lists available at ScienceDirect

Journal of Volcanology and Geothermal Research

journal homepage: www.elsevier.com/locate/jvolgeores

A two-layer model for the evolution and propagation of dense and dilute regions of pyroclastic currents

E.E. Doyle^{a,b,*}, A.J. Hogg^c, H.M. Mader^b, R.S.J. Sparks^b

^a Soil and Earth Sciences Group, Institute of Natural Resources, PN 432, Massey University, Private Bag 11 222, Palmerston North, New Zealand

^b Centre for Environmental and Geophysical Flows, Department of Earth Sciences, University of Bristol, Wills Memorial Building, Queen's Road, Bristol, BS8 1RJ, UK

^c Centre for Environmental and Geophysical Flows, School of Mathematics, University of Bristol, University Walk, Bristol, BS8 1TW, UK

ARTICLE INFO

Article history:

Received 27 July 2009

Accepted 4 December 2009

Available online 16 December 2009

Keywords:

pyroclastic flow
numerical model
dense basal flow
dilute current
sedimentation
deposit

ABSTRACT

We present calculations of a simplified two-layer pyroclastic flow model, which incorporates different physics to represent the dense and dilute regions of column collapse pyroclastic density currents. The two layers evolve separately, but are coupled through mass exchange as suspended ash in the dilute cloud settles into the underlying dense basal layer. The runout distance of the upper dilute current and the associated runout time are found to increase with increasing initial column height and decreasing particle size. Likewise steeper slopes increase the propagation velocity and thus the runout distance. The independent runout distance of the basal flow exhibits opposite behaviour to that of the parent dilute current, increasing with decreasing initial column height and increasing particle size. Observed runout distances can be calculated for basal flows using a Coulomb friction law, but deposit morphology is not well reproduced and is more realistic when an empirical slope-dependent sedimentation rate is included. Dominant flow behaviour is controlled by the rate of mass transfer from the parent suspension current into the dense underflow. Tall column collapses, which contain fine-grained particles, transfer their mass slowly to the dense basal flow and are well described by dilute cloud assumptions. However, for short columns containing coarse grains, the particulate mass is rapidly transferred from the collapsing dilute current into the basal flow. The bulk of the pyroclastic current material propagates as a concentrated suspension for the majority of its travel distance and is better described by the physics of granular avalanches.

© 2009 Elsevier B.V. All rights reserved.

1. Introduction

One of the most hazardous volcanic phenomena is the formation of pyroclastic density currents, generated by the collapse of explosive eruption columns (Sparks and Wilson, 1976), by collapse of lava domes (Mellors et al., 1988; Cole et al., 2002) and by secondary processes when dilute ash clouds interact with topography (Fisher, 1995; Druitt et al., 2002a). Pyroclastic density currents are considered to have two main components, illustrated in Fig. 1 (Sparks et al., 1973; Walker and Wilson, 1983; Valentine and Fisher, 1986). The fundamental paradigm is the development of a two layer structure, first recognised by Lacroix (1904) during observations of the 1902 eruption of Mt Pelée, Martinique. Subsequent research involving both direct observations and investigations of pyroclastic flow deposits has confirmed that this structure often occurs (e.g. Smith, 1960a,b; Sparks et al., 1973; Fisher, 1979; Wilson and Walker, 1982; Valentine and Fisher, 1986; Wilson, 1986; Druitt, 1998). Herein we

characterise a pyroclastic density current as comprising the dense basal part, termed a pyroclastic flow, with high volumetric particle concentrations of tens of %, and an upper dilute turbulent component, termed a pyroclastic surge, with particle concentrations of order of 1% (Druitt, 1998). There is an exchange of mass and heat between these two components leading to a spectrum of flows, from those dominated by the dense part to those dominated by the dilute part (Fisher, 1979; Druitt, 1998).

In the paradigm conceptual model of column collapse, the initial current is dilute and thus the dense basal pyroclastic flow component must develop by mass transfer from the dilute component (Druitt and Sparks, 1982). For example, at Soufrière Hills volcano, Montserrat, columns generated during Vulcanian explosions in 1997 were observed to collapse from heights of 400–750 m. Dilute pyroclastic currents rapidly decelerated and lofted as particles sedimented into the basal regions, resulting in dense basal flows emerging from beneath and moving at tens of m/s until topographic changes brought them to rest (Cole et al., 2002; Druitt et al., 2002b). These basal undercurrents have been documented at numerous volcanoes, including Ngauruhoe, N.Z., Mt. St. Helens, U.S.A., Lascar, Chile and Soufrière Hills, Montserrat (Nairn and Self, 1978; Rowley et al., 1981; Hoblitt, 1986; Levine and Kieffer, 1991; Calder et al., 2000; Cole et al.,

* Corresponding author. Soil and Earth Sciences Group, Institute of Natural Resources, PN 432, Massey University, Private Bag 11 222, Palmerston North, New Zealand.

E-mail address: emmadoyle79@gmail.com (E.E. Doyle).

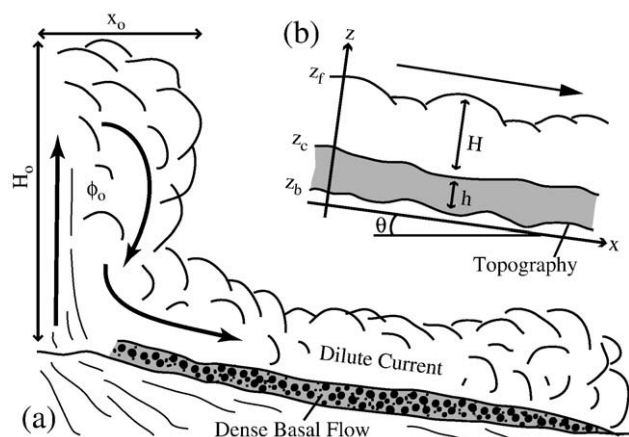


Fig. 1. The pyroclastic flow model. a) A typical eruption column collapse is represented by the release from rest of a constant volume of height H_0 and width x_0 . b) This generates a dilute current of thickness H , propagating down a slope of θ , with x parallel and z perpendicular to the slope. Sedimentation from this turbulent cloud forms a dense basal flow of thickness h (Doyle et al., 2008).

2002; Druitt et al., 2002b; Sparks et al., 2002; Lube et al., 2007a). Upper ash-cloud surges can also be generated from these basal flows, as well as from dome-collapse block-and-ash flows by syn-flow fragmentation and attrition (Dufek and Manga, 2008), and subsequently via shear (Denlinger, 1987), fluidisation (Wilson, 1984) and cold air entrainment at the flow front (Wilson and Walker, 1982). These ash-cloud surges can then detach from the basal flows when the respective flow components respond differently to topography (Fisher, 1995). Further hazardous secondary basal pyroclastic flows, or 'surge-derived' pyroclastic flows, may then be formed due to rapid sedimentation on steep slopes from detached ash-cloud surges and propagate in unexpected directions (e.g. 25th June 1997, Montserrat, Druitt et al., 2002a).

Pyroclastic density currents have commonly been modelled as either dilute turbulent ash suspensions (e.g. Sparks et al., 1978; Bursik and Woods, 1996; Dade and Huppert, 1996; Neri and Macedonio, 1996; Freundt, 1999) or dense pyroclastic flows (e.g. Pitman et al., 2003; Denlinger and Iverson, 2004; Kelfoun et al., 2009). To understand flow transformations between these states, numerical models must couple the dense and dilute regions of these currents and incorporate the interactions between them. Some multiphase models (e.g. Dobran et al., 1993; Neri et al., 2003; Darteville et al., 2004; Dufek and Bergantz, 2007) have been developed to consider the whole spectrum of possible granular concentrations, and related rheologies, within a pyroclastic mixture. However, the numerical integration of these governing equations typically requires a highly resolved mesh and thus a prohibitively large computational effort to simulate flows with a range of initial conditions over realistic length and time scales. To address this, Wadge et al. (1998) and Widiwijayanti et al. (2009) have introduced extensions to map ash-cloud surge impacts beyond the dense basal flow, and Denlinger (1987) and Takahashi and Tsujimoto (2000) have developed two-layer dynamic models for the formation of upper dilute surge clouds from dome-collapse block-and-ash flows.

Direct observations of pumice flows emerging from beneath collapsing dilute currents suggest that the dense basal regions have a distinct interface allowing for independent flow (Cole et al., 1998; Druitt et al., 2002b). The presence of this interface, rather than a gradually varying density profile, is further supported by the observations of surface-wave derived features on pumice flow surfaces of deposits at Lascar volcano (E. S. Calder, personal communication, Nov. 2009). Here we present pyroclastic flow calculations conducted using a two-dimensional two-layer model

that describes both the upper dilute and dense basal regions of these flows with different physics. This model captures both the mass transfer processes occurring during the collapse of volcanic eruption columns and the independent propagation of derived dense basal flows (e.g. at Ngauruhoe in 1975 and Montserrat in 1997). This paper expands upon the study of Doyle et al. (2008) and presents a description of the model, the choice of initial conditions, and implications for flows at Montserrat, W.I. and Ngauruhoe, N.Z. The effects of incorporating an empirical slope-dependent basal sedimentation term are also investigated.

1.1. Modelling philosophy

An emerging debate in geophysics concerns the purpose of models. The model presented here makes several simplifications and is two-dimensional. It is specifically designed to elucidate the principles that govern the formation of dense pyroclastic flows from dilute pyroclastic currents. While large complex numerical simulations certainly have their place, the aleatory and epistemic uncertainties in parameters and the underlying physics are considerable, and the output of such models can be difficult to interpret. Our view is that simplified models have an important role in geophysics in advancing our understanding of the fundamental processes in these complex flows.

2. The two-layer model

A collapsing volcanic eruption column generates a shallow dilute particle suspension current that develops a dense basal flow as it propagates downslope (Fig. 1). Turbulent mixing is assumed to be sufficiently intense to maintain a near uniform volumetric particle concentration in the vertical ϕ (Bonnecaze et al., 1993). Entrainment of ambient air is also neglected, an assumption that is weakest for relatively rapid flows down steep slopes. However, we note that any thickening of the current is balanced by an associated dilution of the suspended particles, so that the buoyancy flux per unit width is conserved. We anticipate that the effects of entrainment could be examined within the framework developed below, but this is not included in this study. The bulk density is denoted $\beta = \rho_s \phi + (1 - \phi) \rho_g$ for mono-disperse solid particles with a density ρ_s suspended in a gas phase of density ρ_g . This density decreases as the well mixed suspended particles settle from the bottom of this layer (Martin and Nokes, 1989) with a settling velocity ω for particles of diameter d given by (Sparks et al., 1997):

$$\omega = \left(\frac{4(\rho_s - \rho_g)gd}{3C_d \rho_g} \right)^{1/2}, \quad (1)$$

where g is gravitational acceleration, and the drag coefficient C_d is herein set to 1 (Woods and Bursik, 1991). The dilute current is initially modelled by equations that describe conservation of mass for the solid [Eq. (2a)] and fluid [Eq. (2c)] phases, and the momentum of the mixture [Eq. (2b)], in which the velocity u , height H , and volume fraction of particulate of the flowing layer evolve both temporally and spatially. The temporal evolution is averaged over turbulent fluctuations. The motion is assumed to be shallow, with vertical lengthscales much smaller than horizontal lengthscales, so that the velocity field is predominantly parallel to the underlying boundary. Conservation of particulate [Eq. (2a)] includes the loss of suspended material by sedimentation to the underlying dense flow. The momentum of the mixture features a balance between the change in the momentum of the flowing layer with the streamwise pressure gradient, downslope gravitational acceleration modified by the presence of basal topography, the momentum lost through sedimentation, and drag due to interaction with the underlying dense layer. The depth-averaged,

isothermal, continuum conservation equations are then given by (Doyle et al., 2008):

$$\frac{\partial(\beta H)}{\partial t} + \frac{\partial(\beta H u)}{\partial x} = -\omega \rho_s \phi \quad (2a)$$

$$\frac{\partial(\beta H u)}{\partial t} + \frac{\partial(\beta H u^2 + (\beta - \rho_a) g \cos \theta H^2 / 2)}{\partial x} = (\beta - \rho_a) g H \sin \theta + (\rho_a - \beta) g \cos \theta H \frac{\partial z_c}{\partial x} - \omega \rho_s \phi u - \beta C_D (u - u_b) |u - u_b| \quad (2b)$$

$$\frac{\partial H}{\partial t} + \frac{\partial(H u)}{\partial x} = 0, \quad (2c)$$

In these equations drag is parameterised analogously to a basal drag, where $C_D = 0.001$ (Hogg and Pritchard, 2004), ρ_a is the ambient density, u_b is the basal flow's depth-averaged velocity, t is the propagation time, and x is the distance along the slope, which is inclined at θ to the horizontal (Fig. 1).

An isothermal average temperature of 850 K is assumed for this dilute flow. Heat transfer to the ground and with the cold ambient air is not considered. Compressibility effects decrease rapidly as the current spreads and thins (Timmermans et al., 2001), and flow velocities are sufficiently low that the current is treated as incompressible. The interstitial ideal gas phase is modelled with a constant density $\rho_g = 0.61 \text{ kg/m}^3$, based on the assumption of a pressure $P = 0.15 \text{ MPa}$.

Particles sedimenting from the base of the depth-averaged, dilute current form the dense basal flow. This basal layer is modelled with rapid granular theory (Savage and Hutter, 1989; Gray et al., 1999; Mangeney-Castelnau et al., 2003), as an incompressible, isothermal, depth-averaged Coulomb continuum (Iverson and Denlinger, 2001; Patra et al., 2005; Kelfoun et al., 2009). We additionally assume that the stress tensor is isotropic (Gray, 2001). Sedimentation from the dilute current above is accommodated by a thickening of the basal flow, as the latter has an assumed constant bulk density $\beta_b = \rho_s \phi_b + (1 - \phi_b) \rho_g$, where ϕ_b is the mono-disperse volume fraction of solids. We neglect the drag at the interface between the basal flow and the upper current (Takahashi and Tsujimoto, 2000), as this is much less than the basal drag with the ground. As of Gray (2001) and Pudasaini and Hutter (2007), we derive depth-averaged equations for a shallow granular flow with mass transfer across the interfaces, leading to the final governing conservation Eq. (22):

$$\frac{\partial h}{\partial t} + \frac{\partial(u_b h)}{\partial x} = \frac{\omega \rho_s \phi}{\beta_b} - L_s \quad (3a)$$

$$\frac{\partial(h u_b)}{\partial t} + \frac{\partial(h u_b^2 + g h^2 \cos \theta / 2)}{\partial x} = g h \sin \theta - \frac{\tau_b}{\beta_b} - g \cos \theta h \frac{\partial z_b}{\partial x} + u_b \left[\frac{\omega \rho_s \phi}{\beta_b} - L_s \right], \quad (3b)$$

The bulk mass conservation Eq. (3a) includes the mass source from the upper current and the mass loss L_s into a deposit, investigated in Section 5.2. Initial calculations neglect L_s to focus only on frictional stopping. In the bulk momentum Eq. (3b), the 1st term on the right hand side is the slope driving force, the 2nd is the basal drag, the 3rd is the acceleration over the basal topography z_b , and the 4th is the momentum contribution due to mass gain or loss. The basal drag is modelled by a Coulomb friction $\tau_b = \text{sgn}(u_b) \beta_b g h \cos \theta \tan \delta$, with a dynamic basal friction angle δ (Pouliquen, 1999).

For both layers, a finite volume numerical method is used to solve the governing equations (Doyle, 2008). The first-order upwind Godunov method is adopted and, for the basal flow [Eqs. (3a) and (b)], the standard shallow-water Roe solver is used to calculate the flux contributions into each numerical cell (Leveque, 2002). Source

terms are then calculated via a fractional step approach. The topographic term of Eq. (3b) is included via the flux difference splitting method of Hubbard and Garcia-Navarro (2000).

For the dilute current [Eqs. (2a)–(c)], it is not possible to find a suitable conservative Roe average state that obeys the required Riemann conditions (Doyle, 2008). Thus we use the alternative 'f-wave' approach (Bale et al., 2003), which guarantees numerical conservation when any linearisation of the governing equations is made, while also incorporating the topographic source terms directly. The initial mass resides on the left hand side of the numerical domain (Fig. 1). The left boundary is treated as a free-slip reflector, while the right boundary is a free-slip outflow. Extensive testing and validation was carried out to ensure the numerical algorithms produced accurate, converged solutions (Doyle, 2008).

3. Initial conditions

3.1. Column collapse height

Initial collapsing fountain conditions are represented by a release of stationary fluid containing a volumetric concentration ϕ_o of particles (Fig. 1). Observations of column collapse heights include the 500–800 m collapses at Mt. St. Helens (Rowley et al., 1981), the c. 500 m collapses during the 1975 eruptions of Ngauruhoe, N.Z. (Nairn and Self, 1978; Sparks et al., 1997), and 400–750 m collapse columns during the 1997 Vulcanian explosions at Soufrière Hills Volcano, Montserrat (Cole et al., 2002). In comparison, large explosive eruptions, such as the Bronze age eruption of Santorini, the 1883 eruption of Krakatau and the 1815 eruption of Tambora, are calculated to have fountain heights of a few km for mass flux rates of 10^8 – 10^9 kg/s (Dobran et al., 1993). Initial conditions for the 2D model are summarised in Table 1a. The chosen range of heights is based on observations, empirical relationships from laboratory experiments (Turner, 1966; Sparks et al., 1997), and multiphase column collapse simulations (Dobran et al., 1993; Neri and Dobran, 1994; Giordano and Dobran, 1994; Clarke et al., 2002).

In all 2D calculations, we consider an instantaneous, constant volume, column collapse. The half-width of the column x_o (Fig. 1) is found from an assumed aspect ratio of $a = 3$, where $a = H_o/x_o$, selected from the value of 4 suggested by Dobran et al. (1993) and the range of 2–3 inferred from simulations by Clarke et al. (2002). Although this initial aspect ratio is relatively high, we apply the shallow layer model to describe the motion. This may be inaccurate during the very initial stages, where there may be relatively high vertical accelerations, but will soon capture the dynamics when the flow has evolved away from the initial conditions.

3.2. Initial volume concentrations and particle sizes

The particle concentration in collapsing eruption columns is dependent upon several factors, including the gas content, mass eruption rate, vent diameter, and entrainment rate (e.g. Sparks et al., 1978; Wilson et al., 1980; Bursik and Woods, 1991; Giordano and Dobran, 1994; Neri and Dobran, 1994; Clarke et al., 2002; Carazzo and Kaminski, 2006). We adopt initial mono-disperse particle volume concentrations of $\phi_o = 0.01$ and 0.005, to cover a typical range of values inferred from these modelling and empirical studies. Future simulations could consider higher concentrations for the smallest, highly unsteady, column collapse fountains. The grain size variations observed in ignimbrites (Walker, 1971; Sparks, 1976) and in tephra fall deposits (Kaminski and Jaupart, 1998) indicate that explosive eruption columns have a very wide range of grain sizes. Further, individual deposits can be dominated by coarse or fine grains. We model mono-disperse grain sizes from 50 cm to 125 μm (Table 1b). Using empirical information on tephra particle densities to constrain typical values, we assume that particle density ρ_s decreases monotonically with increasing diameter d ,

Table 1
a) Initial heights H_o and half-widths x_o of the collapsing column inferred for expected vent ejection velocities W . b) Corresponding particle sizes d , solids densities ρ_s and calculated bulk densities β_o . Initial volume concentrations of $\phi_o = 0.005$ and 0.01 and gas density $\rho_g = 0.61 \text{ kg/m}^3$ are assumed. Settling speeds ω are calculated using a high Reynolds settling velocity [Eq. (1)]. Example initial masses are shown for those simulations that consider $\phi_o = 0.01$, assuming the 2D column has unit breadth.

a)								
Vent velocity, W	H_o	x_o						
m/s	m	m						
50	150	50						
100	550	183						
150	1100	367						
200	1600	533						
b)								
Diameter, d	ρ_s (kg/m^3)	β_o , (kg/m^3)		ω (m/s)	mass for $\phi_o = 0.01$ ($\times 10^4 \text{ kg}$)			
		$\phi_o = 0.01$	0.005		$H_o = 150$	550	1100	1600
–	–	–	–	–	–	–	–	–
125 μm	2400	24.6	12.6	2.52	18	248	992	2099
500 μm	2000	20.6	10.6	4.61	15	208	831	1758
1 mm	1750	18.1	9.4	6.1	14	183	730	1545
2 mm	1500	15.6	8.1	8.0	12	157	629	1331
8 mm	1000	10.6	5.6	13.1	8	107	428	905
16 mm	800	8.6	4.6	16.5	6	87	347	734
5 cm	800	8.6	4.6	29.2	6	87	347	734
10 cm	800	8.6	4.6	41.2	6	87	347	734
50 cm	800	8.6	4.6	92.3	6	87	347	734

from 2500 kg/m^3 for a $125 \mu\text{m}$ particle to 800 kg/m^3 for particles above 16 mm (Giordano and Dobran, 1994; Freundt, 1999).

3.3. Other parameters

The maximum packing fraction of uniform sized spheres is 0.74 (see Dobran et al., 1993). However, fluidisation would reduce this value. We assume a bulk volumetric particle concentration of $\phi_b = 0.5$ for the dense basal flow, consistent with field estimates (Sparks, 1976; Druitt, 1998) and mid range between the values of 0.4 and 0.6 used by Denlinger and Iverson (2001), for flows at Mt. St. Helens and debris avalanches, respectively. Basal flow emplacement is controlled by a Coulomb basal friction law (Pouliquen and Forterre, 2002; Mangeney et al., 2000) with an assumed constant friction angle of $\delta = 10^\circ$, which is typical for small, dense, flows that typically start to deposit on slopes of 6 – 10° (Sparks et al., 1997; Freundt, 1999; Druitt et al., 2002b; Roche et al., 2004). We note that this should be viewed as a bulk friction parameter that is only indirectly related to the microscopic friction angle measured at particle scales.

Following standard practice for shallow-water numerical solvers (e.g. Mangeney-Castelnau et al., 2003), we impose further conditions to locate the front of the flows. The dilute current front $x_{\beta F}$ is defined where the bulk density equals that in the ambient β_a , which has a volumetric particle concentration of $\phi_a = 10^{-8}$. The dilute current calculations then continue until its average bulk density $\tilde{\beta}$ is within 10% of this ambient. Assuming a value of 5% or 15% has little effect on the dilute current runout (Doyle, 2008). The dense basal front x_{gf} is defined where the height h reduces to $100 \mu\text{m}$, which is less than the smallest grain size considered here. For both numerical layers, runout distances differ by $<0.5\%$ for grids of 2 or 5 m . Thus, calculations with initial collapsing column heights of $H_o \leq 1100 \text{ m}$ use 2 m cells, and calculations with taller columns use 5 m cells (Doyle, 2008).

3.4. Topographic profiles

Benchmark model calculations cover a range of representative volcanic cone topographies. These include a full set of initial conditions explored on a slope inclined at $\theta = 13^\circ$ for 10 km flanked by a 1° plateau to 25 km (Table 1 and Fig. 2a). In addition, a subset of these initial conditions has been conducted on slopes of $\theta = 2^\circ$ to 30°

extending to 7 km , to investigate the effect of the cone diameter and inclined slope angle. These include 550 m columns with $\phi_o = 0.01$ and $d = 1 \text{ mm}$ and 5 cm . Finally, models with $H_o = 550 \text{ m}$, $\phi_o = 0.01$, and $d = 1 \text{ mm}$ to 50 cm have been conducted on profiles typical of the northern slope of Soufrière Hills, Montserrat and Ngauruhoe, N.Z., illustrated in Fig. 2b. Both these topographies consider basal friction angles from $\delta = 2^\circ$ to 35° , encompassing the most fluidised flows (Freundt, 1999) and those that are dominated by granular avalanche type behaviour (Nairn and Self, 1978).

Calculated flow runouts are then compared in Sections 4 and 5 to observed runout distances during the 1997 Vulcanian eruptions of Montserrat, W.I. and the 1975 eruptions of Ngauruhoe. At Montserrat, discharge volumes were typically 1.9 – $3 \times 10^5 \text{ m}^3$ DRE, with clasts up to 30 cm in a poorly sorted matrix ($<32 \text{ mm}$, Druitt et al., 2002b; Cole et al., 2002). The Ngauruhoe eruptions produced 1 – $1.5 \times 10^6 \text{ m}^3$, with individual flows $<5000 \text{ m}^3$ and a bimodal grain size distribution (matrix: 16 and $375 \mu\text{m}$; clasts: $65\% > 2 \text{ mm}$ and $58\% > 32 \text{ mm}$, Nairn and Self, 1978; Lube et al., 2007a).

4. The collapsing eruption column

4.1. Example column collapse

Following column collapse, the dilute current propagates until all its mass is transferred to the basal flow. Initially the dense basal flow front x_{gf} is coincident with the dilute current front, $x_{\beta F}$, illustrated in Fig. 3. When the dilute current has terminated, the basal flow has a wedge shaped morphology thinning towards its front. If the dilute current has terminated on the volcanic slope with an inclination angle θ exceeding that of the basal friction angle of the basal flow δ , then it can continue to propagate. The thicker material at the back of the flow has a greater velocity, and thus catches up with the flow front and propagates beyond the maximum runout of the upper dilute current (Fig. 3). This basal flow reaches its maximum velocity when it reaches the plateau. It then propagates onto this plateau, and eventually comes to rest due to friction. For example, on the 7 km , 15° cone, the dilute current from a 550 m column, with 1 mm particles at a concentration of $\phi = 0.01$, will terminate at 3.2 km from the vent. However, the basal flow continues to 11.6 km (Fig. 3). Conversely, if the dilute current terminates on the plateau, friction prevents

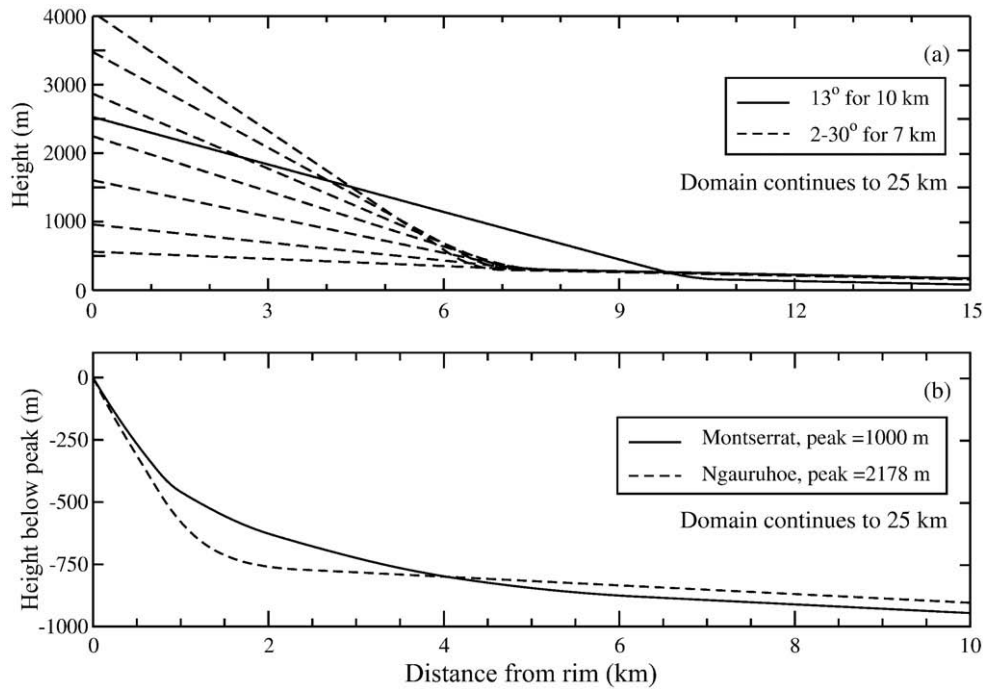


Fig. 2. a) The synthetic topographies considered. All flanked by a 1° plateau to 25 km. b) The slope profiles at Montserrat and Ngauruhoe. For Montserrat, the average of the northern slope of Soufrière Hills volcano is used. For Ngauruhoe, the profile quoted by Lube et al. (2007a) is used. The height axis corresponds to the height below the peak. A slope angle of 1° is assumed beyond 6 km.

the dense basal flow from moving beyond the dilute current (Doyle et al., 2008).

4.2. Controls on runout distance

The dilute current runout, $x_{\beta F}$, increases as grain size d decreases and column height H_o increases. Sedimentation of particles reduces the density difference between the dilute current and the ambient, resulting in deceleration. The relationship between runout $x_{\beta F}$, grain size, and initial column height is found empirically to be given by:

$$\frac{x_{\beta F}}{\alpha x_o} = [0.36 \pm 0.04] \left(\frac{\phi_o H_o}{d} \right)^{[0.32 \pm 0.02]}, \quad (4)$$

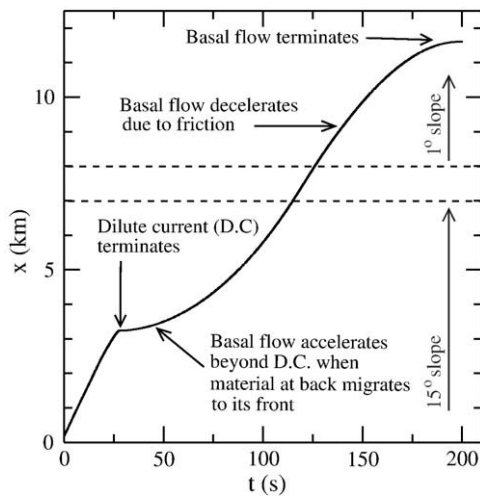


Fig. 3. An example of modelled pyroclastic current behaviour, for the case where the dilute current passes all its mass to the basal flow before the plateau. $H_o = 550$, $d = 1$ mm, $\phi = 0.01$, conducted on a 15° slope extending to 7 km. Horizontal dashed lines indicate the gradual change between this slope and the 1° plateau.

for the 13°, 10 km cone (Fig. 4a). On the 15°, 7 km cone, the exponent α is 0.33 and the proportionality constant K is 0.35. Increasing the 7 km slope angle from 15° to 30° increases the runout by 18% for a current with 1 mm particles and 4% for a current with 5 cm particles. The exponent α in Eq. (4) increases from 0.29 to 0.36 as slope angle increases from 2° to 30° (Table 2). Similar values are found for the 550 m model column collapses with topographic profiles from Montserrat and Ngauruhoe (Fig. 4b).

4.3. Controls on runout time

The runout time, $t_{\beta F}$ increases with decreasing particle size d and increasing column height H_o . By considering the scaling parameter $\phi_o H_o / d$ used in Eq. (4), and the initial reduced gravity $g'_o = g(\beta_o - \rho_a) / \beta_o$ of the column, the runout time on the 13°, 10 km cone, collapses to two relationships:

$$\frac{t_{\beta F}}{(x_o / g'_o)^{0.5}} = [0.73 \pm 0.06] \left(\frac{\phi_o H_o}{d} \right)^{[0.25 \pm 0.01]} \quad (5a)$$

$$\frac{t_{\beta F}}{(x_o / g'_o)^{0.5}} = [0.4 \pm 0.1] \left(\frac{\phi_o H_o}{d} \right)^{[0.4 \pm 0.1]} \quad (5b)$$

for values above and below approximately $\phi_o H_o / d \approx 100$ (Fig. 5a and Table 2). These two different regimes reflect the assumed non-uniform relationship between particle size d and density ρ_s (Table 1).

The dilute runout time of small volume columns on the 15°, 7 km cone, confirms relationship [5a] with an exponent $\alpha = 0.25$ and a proportionality constant K of 0.74. The exponent α increases from 0.23 to 0.28 as the slope angle increases from 2° to 30° (Table 2). Similar values are found for the 550 m model column collapses on topographic profiles from Montserrat and Ngauruhoe, illustrated in Fig. 5b. Exponents found for these “real world” topographies are closer to those found for the 30° volcanic cone than the 2° slope (Table 2).

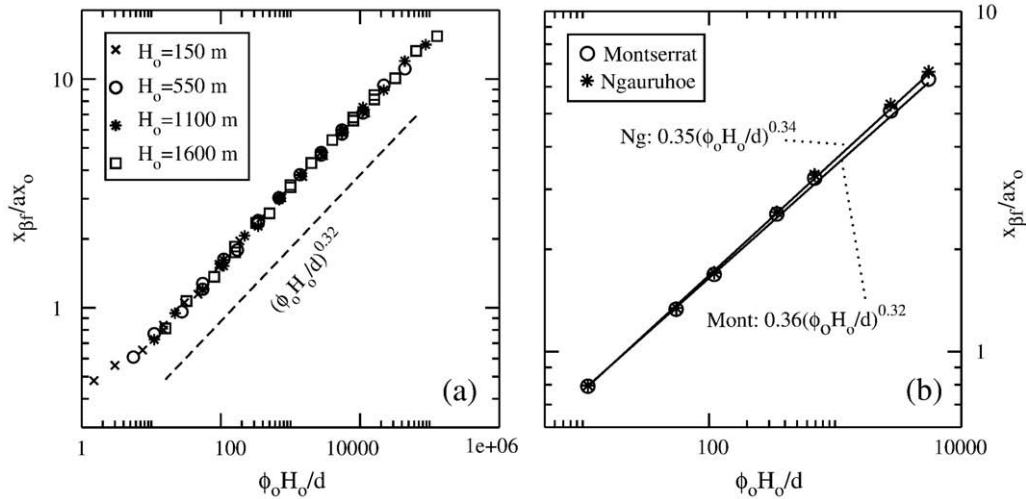


Fig. 4. The relationship between the upper dilute current runout distance $x_{\beta F}$ with respect to the initial conditions of the collapsing column, considering x_o , H_o , aspect ratio a , particle size d and the volumetric particle concentration ϕ_o . a) For a cone of $\theta = 13^\circ$ to 10 km, and b) the profiles of Montserrat and Ngauruhoe (Section 3.4).

4.4. Controls on velocity

The upper dilute currents initially accelerate downslope, and then decelerate due to mass transfer into the basal flow (Fig. 6a). Currents containing coarser particles decelerate soon after onset (Fig. 6b). Initial collapsing currents at Montserrat had frontal velocities of 30–60 m/s (Cole et al., 2002; Druitt et al., 2002a,b). The maximum velocities calculated for models of small volume flows on the Montserrat topography are much higher, ranging from 97 m/s to 136 m/s (Fig. 6c). However, after this maximum there is a rapid deceleration in the front velocity. Models with particles between 8 mm and 5 cm calculate dilute current runout distances (Section 4.2) and late stage front velocities comparable to those observed.

The higher initial velocities in the models are attributed to the simplified 2D model and its instantaneous, constant volume, column collapse. An axisymmetric model includes radial spreading which would slow the flow considerably. However, many of the observed radially collapsing pyroclastic columns rapidly become channelised on the volcanic flanks, where a 2D model is suitable. The idealised initial condition considers an instantaneously formed column, released from rest. This produces currents with initial propagation velocities proportional to the initial column height. These velocities are likely to be higher than those produced from a gradually collapsing column. However, after this initial adjustment phase, the propagation velocities away from source are controlled by dynamic balances independent of this initial velocity scale.

4.5. Reconsidering these scaling results

The scaling results for the runout distance and time given in Eqs. (4), (5a) and (5b) may be rationalised as follows: the time-scale for the particles to settle through the layer, t_{∞} , is given by H_{∞}/ω , where H_{∞} is a typical depth scale and ω is the particle settling velocity. On the assumption that throughout its motion the dilute current is accelerated down the slope under gravity, an estimate for the downslope length-scale, x_{∞} , is given by $x_{\infty} \sim g'_o \sin \theta t_{\infty}^2$, where g'_o is the initial reduced gravity given by $g'_o = g(\beta_o - \rho_a)/\beta_o$. Conservation of fluid volume implies that $H_{\infty} x_{\infty} \sim A$, where A is the initial volume per unit width. Recalling that $a = H_o/x_o$ we identify $A = H_o x_o = H_o^2/a$, and find that

$$\frac{x_{\infty}}{H_o} \sim \left(\frac{g'_o \sin \theta H_o}{a^2 \omega^2} \right)^{1/3}, \tag{6}$$

$$t_{\infty} \left(\frac{g'_o \sin \theta}{H_o} \right)^{1/2} \sim \left(\frac{g'_o \sin \theta H_o}{a^2 \omega^2} \right)^{1/6}. \tag{7}$$

We can simplify these expressions further by substituting for the initial reduced gravity g'_o into the settling velocity $\omega^2 \sim (\rho_s - \rho_g)gd/(C_d \rho_g)$, where the constant 4/3 has been neglected from the definition of ω to focus on the dimensional terms. We further note that since ρ_g

Table 2
The non-dimensional relationships found for the upper dilute current runout distance $x_{\beta F}$ and the runout time $t_{\beta F}$. All relationships are dependent on the initial column height H_o , which is composed of particles of size d at an initial volumetric concentration ϕ_o . Other nomenclature: the initial column half-width x_o , the distance to the shallow plateau slopes x_{plat} , the initial aspect ratio of the column $a = H_o/x_o$ and the gravitational acceleration g .

Non-dimensional relationship: $Y = KX^\alpha$ where $X = (\phi_o H_o/d)$						
x_{plat}	θ°	δ°	Dependent Y	K	α	notes
10 km	13	10	$x_{\beta F}/ax_o$	0.36 ± 0.04	0.32 ± 0.02	Eq. (4). N.B: $a = 3$
7 km	2	2–35		0.40	0.29	
7 km	30	2–35		0.31	0.36	
Montserrat			$t_{\beta F}/(x_o/g'_o)^{0.5}$	0.36 ± 0.01	0.33 ± 0.01	Eq. (5a), $X > 100$ Eq. (5b), $X < 100$ for $X > 100$ for $X > 100$
Ngauruhoe				0.35 ± 0.01	0.34 ± 0.01	
10 km	13	10	0.73 ± 0.06	0.25 ± 0.01		
10 km	13	10	0.4 ± 0.1	0.4 ± 0.1		
7 km	2	2–35	0.83	0.23		
7 km	30	2–35	0.60	0.28		
Montserrat				0.90 ± 0.06	0.25 ± 0.01	$X > 100$
Ngauruhoe				0.82 ± 0.05	0.26 ± 0.02	$X > 100$

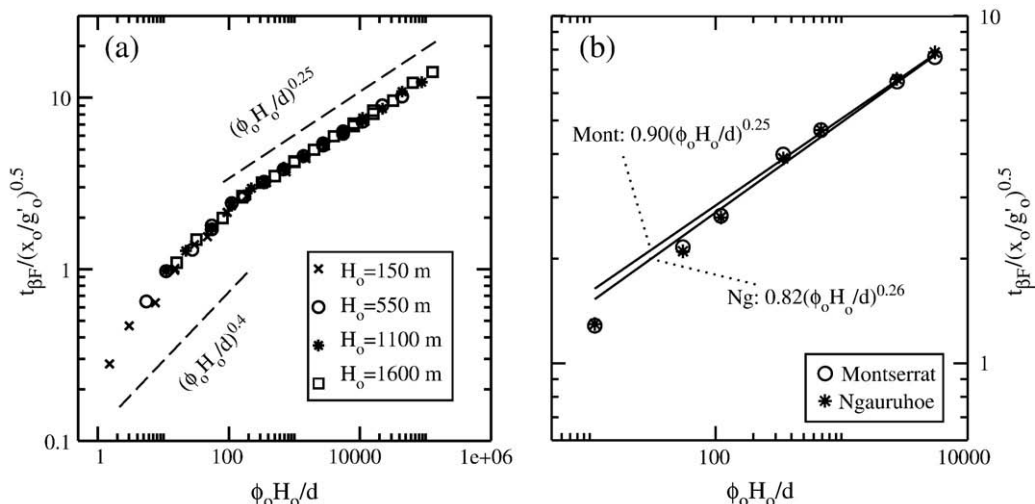


Fig. 5. Relationship between runout time $t_{\beta F} / (x_0 / g_0')^{0.5}$ and proposed scaling parameter $\phi_0 H_0 / d$ using the initial reduced gravity $g_0' = g(\beta_0 - \rho_a) / \beta_0$. a) For a cone of $\theta = 13^\circ$ to 10 km, and b) the profiles of Montserrat and Ngauruhoe (Section 3.4).

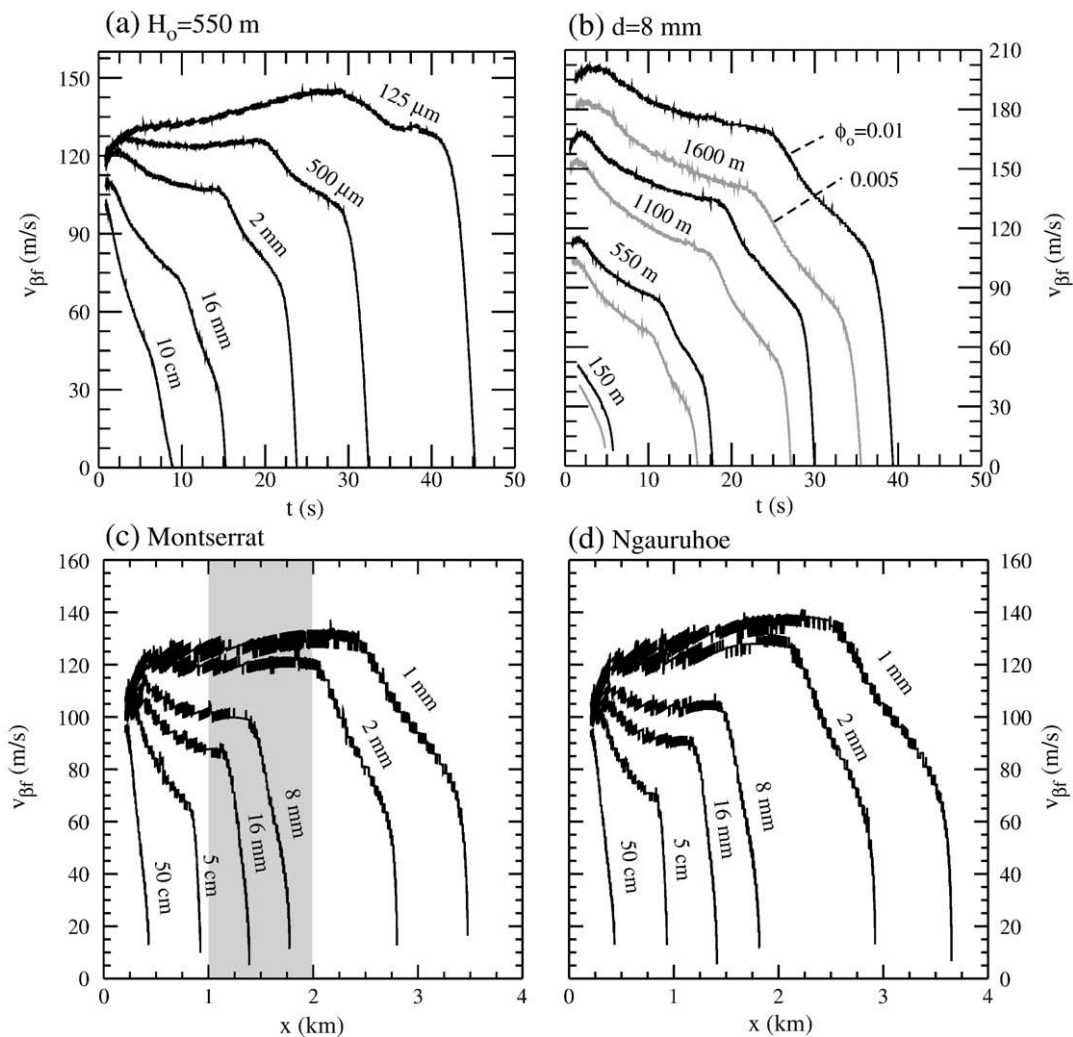


Fig. 6. a) The velocity of the upper dilute current front as a function of time after release for $H_0 = 550$ m and varied particle size, as indicated. b) For $d = 8$ mm and varied initial column heights as shown. c and d) The corresponding velocity calculated on the typical Montserrat and Ngauruhoe profiles (Section 3.4) as a function of distance. All black lines represent values for volumetric particle concentrations of $\phi_0 = 0.01$ and grey lines on (b) are examples for a lower initial volume concentration of 0.005. The grey box in (c) indicates the range of observed maximum runouts for column collapse dilute surges at Montserrat (Druitt et al., 2002b). Note that the velocity is estimated by taking a central difference of the front position across each time step and averaging across adjacent 20 time step windows. The localised variations in velocity are not due to numerical instabilities, but are rather errors in numerically estimating the gradient from the grid resolution of the front position. Approximate errors of ± 6 m/s are estimated for all velocities.

and ρ_a are 0.61 and 1.29 kg/m³ respectively, while ρ_s is of the order of 10³ kg/m³ then $(\rho_s - \rho_g)/(\rho_s - \rho_a) \sim 1$. Thus, we find that

$$\frac{g'_o}{\omega^2} \sim \frac{\phi_o C_d \rho_g}{d \beta_o} \quad (8)$$

Substituting this into the scaling relationships above [Eqs. (6) and (7)] yields

$$\frac{x_\infty}{ax_o} \sim \left(\frac{C_d \rho_g \sin \theta}{\beta_o a^2} \right)^{1/3} \left(\frac{\phi_o H_o}{d} \right)^{1/3} \quad (9)$$

and

$$\frac{t_\infty}{(x_o/g'_o)^{1/2}} \sim \left(\frac{C_d \rho_g a}{\beta_o \sin^2 \theta} \right)^{1/6} \left(\frac{\phi_o H_o}{d} \right)^{1/6}, \quad (10)$$

which are of a similar form to that found empirically and given by Eqs. (4) and ((5a),(b)). The dependence of the proportionality constant on slope angle agrees with model calculations for relationship [10], but not for [9] (see Table 2).

5. The derived dense basal flow

Each basal flow starts to propagate independently at different distances from the vent, depending on the runout distance of the upper dilute current $x_{\beta F}$. This independent travel distance decreases with increasing initial column height and decreasing particle size, reflecting the controls on the dilute current runout. For those basal flows that stop within the 25 km computational domain (Fig. 7a), the runout x_{GF} increases with the inclined slope angle of the 7 km cone (Fig. 7b). For a basal friction angle of $\delta = 10^\circ$, the runout almost doubles as the slope angle θ increases from 15° to 30° . In turn, the runout of the basal flow increases with decreasing friction angle. On slopes of $\theta = 30^\circ$, flows with $\delta = 10^\circ$ propagate almost three times further than flows with $\delta = 25^\circ$, due to their greater potential energy. Increasing θ/δ not only increases both the basal flow runout and that of the parent dilute current (Section 4.2), but also increases the relative distance between them (Fig. 7c and d). An increase of θ/δ results in a greater increase of the basal flow's momentum, compared to that of the dilute current, because of the relative decrease in the basal friction defined by δ .

Basal flows produced by small volume column collapses at Ngauruhoe have been observed to terminate at distances of 0.8–2.2 km (Nairn and Self, 1978; Lube et al., 2007a). At Montserrat, corresponding flows stop at distances of 3–6 km from source. The longer runouts observed at Montserrat may be due to greater

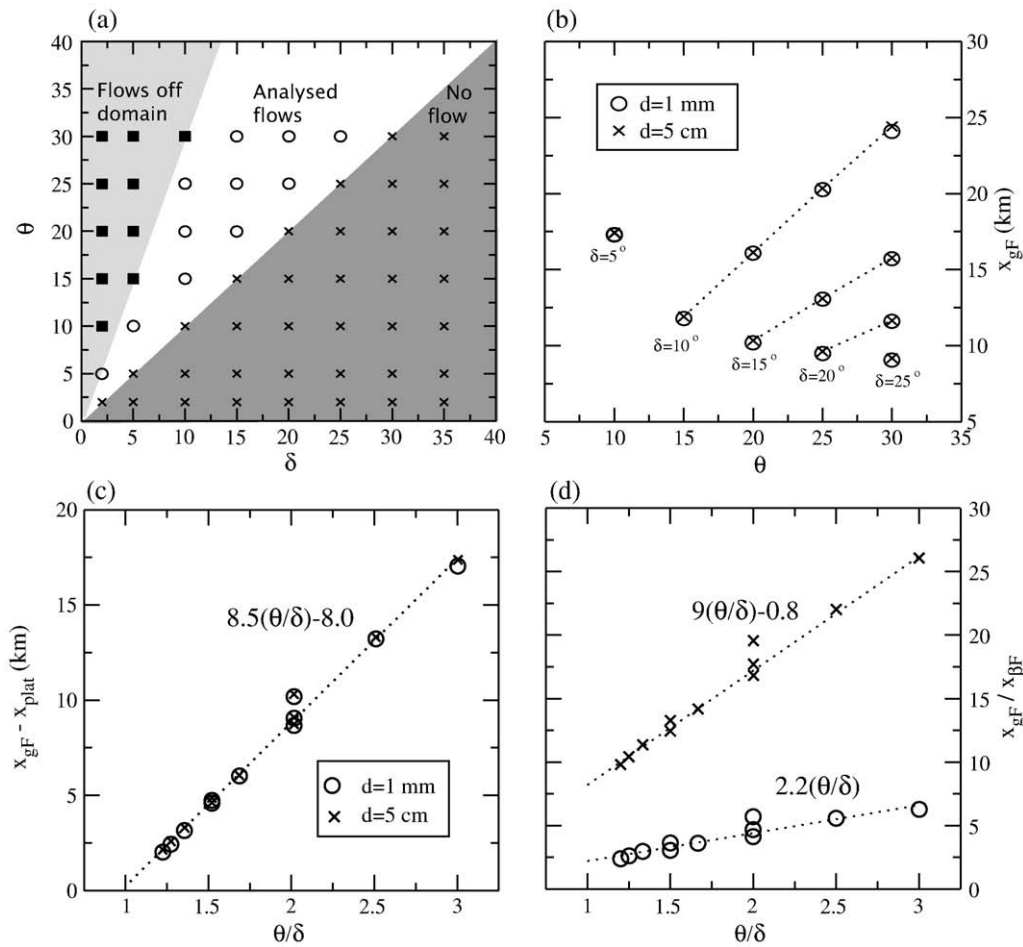


Fig. 7. a) Schematic chart indicating modelled flow behaviour as a function of the volcanic cone slope angle θ and basal friction angle δ . The dense basal flows either flow off the computational domain (light grey shading), do not flow beyond the upper dilute current (dark grey shading), or flow down the volcanic slope to stop on the plateau (no shading). We focus on the latter group in the analysis discussed in Section 5. b) The runout of the basal flow x_{GF} , as a function of θ for various δ , for $d = 1$ mm and 5 cm. c) The distance between x_{GF} and the start of the plateau x_{plat} , as a function of the ratio θ/δ . d) The ratio between x_{GF} and the runout of the upper dilute current $x_{\beta F}$, as a function of θ/δ . The multiple data points at $\theta/\delta = 1.5$ and 2 in (c) and (d) correspond to the multiple combinations of the analysed values of θ and δ that produce these values of θ/δ (a). Longer runouts are found for lower δ in the constant values of θ/δ .

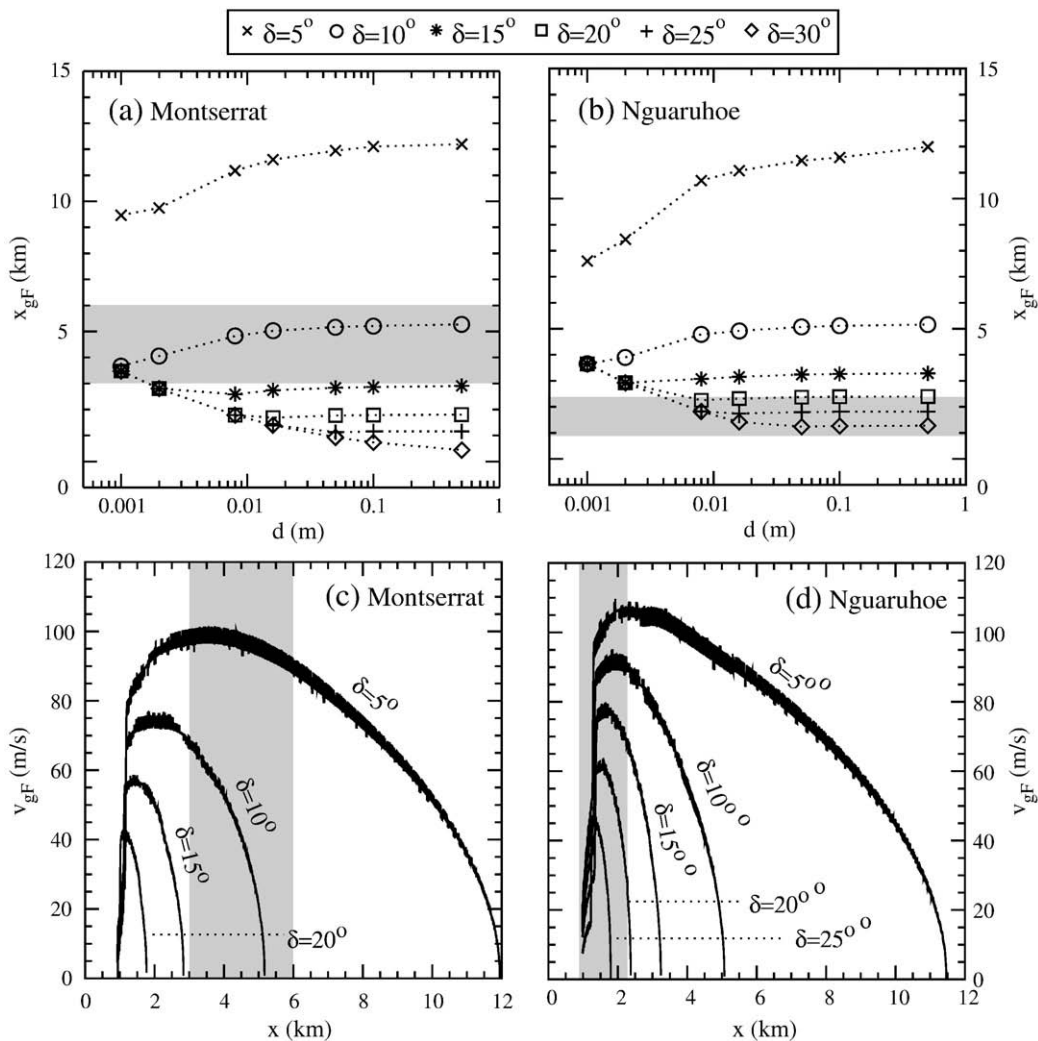


Fig. 8. a) The maximum distance reached by the basal flow with respect to d at Montserrat for various basal friction angles δ , and b) at Ngauruhoe. c) Example front velocities of the basal flow for varied basal friction angles, with $d = 5$ cm at Montserrat, and d) at Ngauruhoe. Grey boxes represent the observed range of runout distances (Druitt et al., 2002b; Lube et al., 2007a).

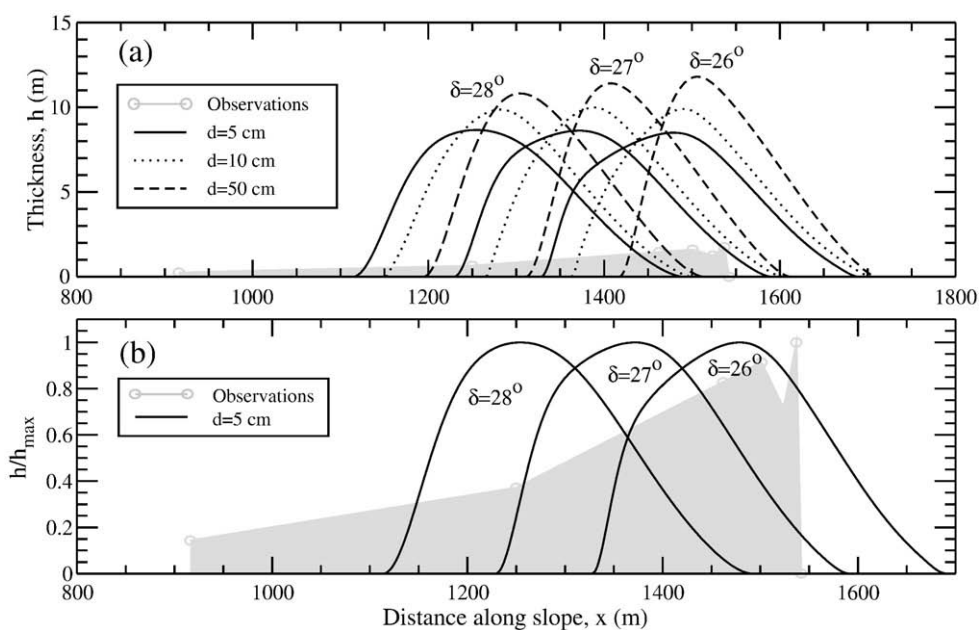


Fig. 9. a) Examples of basal flow deposit, for values of δ and d that produce runout distances comparable to the Unit II-S2 deposit at Ngauruhoe (grey shading, Lube et al., 2007b) b) Same observations, normalised to the deposit maxima to highlight morphological differences.

fluidisation of the basal flow, which reduces basal friction (Roche et al., 2002). Indeed, assumed lower friction angles capture the runout distances on the Montserrat topography, compared to the higher values required for the Ngauruhoe topography (Fig. 8a and b).

The calculated propagation velocity increases with decreasing basal friction angle (Fig. 8c and d). Coarser particles are passed from the dilute current to the basal flow closer to the vent than fine particles. Thus the basal flow forms on these steeper slopes with a higher initial momentum. Calculated velocities are thus much higher on the steep slopes close to the vent than those on the shallow slopes far from source (Fig. 8c and d). A modelled flow on the Ngauruhoe topography, with $\delta = 20\text{--}25^\circ$, has a calculated velocity of 30–60 m/s within 2 km of the source, decelerating to rest on the plateau. This behaviour is comparable to that inferred from depositional evidence, which suggests velocities of 30 m/s on steep upper slopes and 10 m/s on shallow inclines (Lube et al., 2007a).

5.1. The final basal flow deposit

Model calculations of 550 m columns with basal friction angles of $\delta = 27 \pm 1^\circ$ produce runout distances comparable to that of the 1975 Unit II-S2 deposit at Ngauruhoe (Fig. 9a and Lube et al., 2007b). However, the modelled deposit thickness is much greater than that observed. This is most likely due to differences between the modelled and real mass of the Ngauruhoe deposits. In addition, the models do not capture realistic deposit morphologies. They have a central maxima with an unrealistically high aspect ratio (Fig. 9b). If poly-dispersed grain size distributions were introduced into the model, coarse grains could be expected to deposit closer to the source than fine grains. If these fine grains comprise the larger volumetric component, then an initially wedge shaped flow could be produced. However, the assumed Coulomb friction only stops the flow when the frictional drag exceeds the momentum of the flow, when $\theta < \delta$. Thus, shortening of the flow also occurs, as material at the back catches up with the front. Deposits are thus not modelled until 1.2 km from source, contrary to observed deposit formation on steep slopes from 0.7 km (Lube et al., 2007a).

5.2. Alternative stopping regimes

Static and flowing regions play a vital role in deposit formation from laboratory granular flows (Lube et al., 2007b), as the interface between them consumes the flowing layer. Static deposit growth is envisaged to occur via a thin high shear region at this interface. This deposit grows at 0.33 m/s during free fall of the column and 0.15 m/s during the subsequent later flow. The shape and runout of these laboratory flows can be successfully modelled using a constant Coulomb friction with a constant sedimentation rate (Doyle et al., 2007).

Incorporating an equivalent sedimentation into the basal flow model can explain the longer, thinner, deposits observed for real flows compared to model calculations (Fig. 9b). Applying a constant basal sedimentation L_s [Eqs. (3a) and (b)] of 0.15–0.20 m/s captures observed Ngauruhoe runouts when $\delta = 15^\circ$, for particles of 5 cm (Fig. 10a). However, the final deposit is still not realistic, with deposit formation on the very steepest slopes closest to the source. Lube et al. (2007a) estimate sedimentation rates of 0.05 m/s on Ngauruhoe slopes of $\theta = 20^\circ$ and c. 0 m/s above 30° . Thus, any numerical description must capture the negligible sedimentation when $\theta > \delta$, as well as its increase with δ/θ . We suggest:

$$L_s(\theta) = \begin{cases} L_s^0 \left(1 - \left|\frac{k\theta}{\delta}\right|\right) & \text{if } (1 - |k\theta/\delta|) \geq 0 \\ 0 & \text{otherwise} \end{cases} \quad (11)$$

where L_s^0 is the sedimentation rate on the horizontal, and the empirical value $k = \delta/31^\circ$ forces the observed deposit free region at

$\theta = 31^\circ$. We acknowledge this empirical function requires further verification.

Modelled deposits produced with Eq. (11) have more realistic morphologies (Fig. 10b). Increasing the friction angle shortens and thickens the deposit. Increasing L_s^0 results in only a minor decrease in runout (Fig. 10c and d). Assuming a basal friction angle of $\delta = 27 \pm 1^\circ$ results in deposits with runout distances comparable to observations. However, the modelled deposits are still too thick. This is most likely due to uncertainties in the initial conditions. Models that consider a smaller initial mass calculate more realistic deposits, with similar front positions (Fig. 10e). Thus, by incorporating an empirical slope-dependent sedimentation rate, both the runout and morphology of observed deposits can be modelled. This is not possible when a simple Coulomb friction stops the flow.

6. Summary and conclusions

Conceptual transport models identify two end-member structures for pyroclastic density currents (see Section 1 and Sparks et al., 1973; Fisher, 1979; Walker and Wilson, 1983; Fisher and Schmincke, 1984; Valentine and Fisher, 1986; Cas and Wright, 1987). In one end member, mass transfer is slow and the bulk of material is transported in a dilute turbulent pyroclastic surge (e.g. Branney and Kokelaar, 1992; Dade and Huppert, 1996). Transport is dominated by the dilute turbulent suspension with concentrations of c. 1% and propagation velocities of tens to hundreds of m/s. Deposits are fine-grained, can display cross-bedding and typically mantle topography. In the other end member, mass rapidly transfers from the dilute collapsing eruption column to form a dense basal flow (e.g. Sparks, 1976; Wright and Walker, 1981; Wilson, 1985) which dominates the pyroclastic flow. The basal flows have concentrations of c. 50% and propagate at velocities of a few to tens of m/s, with theoretical models suggesting speeds of up to 250 m/s in the largest flows (Sparks et al., 1978). Transport is dominated by particle interactions and gas fluidisation, and these flows are inferred to have an interface above which the solids concentration rapidly decreases (e.g. Sparks, 1976; Druitt, 1998).

Both end-member behaviours may occur in one flow (Valentine, 1987; Druitt, 1992; Palladino and Valentine, 1995; Hughes and Druitt, 1998; Branney and Kokelaar, 2002; Darteville et al., 2004), with the dominant behaviour (Valentine, 1987) controlled by mechanisms including changes in topography and the mass transfer rate from the upper dilute current (Freundt and Schmincke, 1985; Fisher, 1990; Branney and Kokelaar, 1997; Druitt, 1998; Browne and Gardner, 2005). Evidence of lateral changes in the deposits can be used to infer changes to the character of the flow with time and distance. For example, proximal lag breccias and cross-stratified surge deposits have been interpreted as being formed when the flow is in an initial expanded and dilute state, while lateral changes to massive layer 2 deposits suggest transformation to predominantly dense flows with distance (Druitt and Sparks, 1982; Calder et al., 2000). Observations of collapsing columns (Cole et al., 2002; Druitt et al. 2002a, and Section 1) suggest that this behaviour may be typical for some volcanoes.

The primary strength of the two-layer model presented here is that incorporating the different physics of the dense and dilute regions of a pyroclastic density current allows us to explore the complex interactions between the two layers and relate propagation characteristics observed in the field to initial and flow conditions.

We find that the runout distance and time of the dilute current decreases with increasing particle size, and increases with increasing column height and particulate volume concentration. The runout of the derived basal flow behaves in an opposite manner, increasing with decreasing column height and increasing particle size. The shorter upper dilute current runout distances found for these conditions result in greater downslope distances over which the derived basal

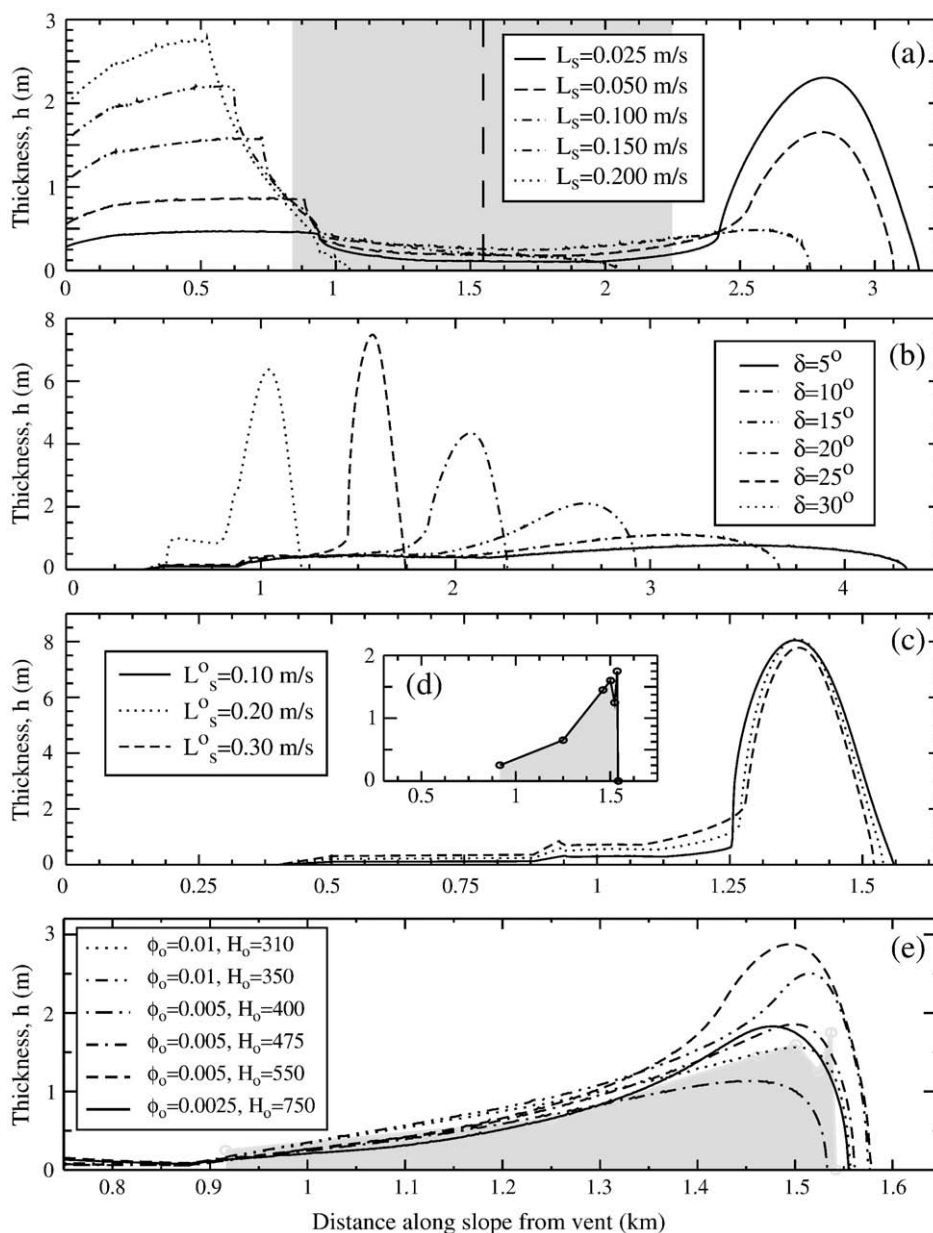


Fig. 10. a) Examples of the deposit produced with a constant empirical sedimentation rate L_s , for $\delta = 15^\circ$ and $d = 5$ cm. The grey box indicates the range of front positions observed at Ngauruhoe, and the vertical dashed line is the maximum deposit distance for Unit II-S2 (Lube et al., 2007a). b) Deposit produced with a slope-dependent sedimentation rate $L_s(x)$ [Eq. (11)], assuming $L_s^o = 0.15$ m/s, $d = 5$ cm and various δ , and c) for $\delta = 27^\circ$ and various L_s^o . d) (inset to c) The observed Unit II-S2 deposit at Ngauruhoe (Lube et al., 2007a). e) The deposit produced using $L_s(x)$ [Eq. (11)] with $L_s^o = 0.30$ m/s, $\delta = 26^\circ$, $d = 5$ cm, and smaller mass in the initial column.

flows can independently propagate and gain momentum. This basal flow is then primarily controlled by the slope and basal friction angles. These results indicate that the eruption column height and fragmentation dynamics (defined by the grain size), dictate the dominant flow type for pyroclastic currents. Topography, and the granular properties of the basal layer, then control the relative runout of the flows. Including an empirical slope-dependent sedimentation rate (Section 5.2) results in more realistic deposits.

The runout behaviours are associated with the rate of mass transfer between the upper and lower layers. The time taken for mass to transfer into the basal flow decreases with increasing particle size (Fig. 11a, Table 1b). For illustration, a 550 m column with 10 cm particles transfers the majority of its mass (75%) within 8 s and 0.8 km (Fig. 11a and b). Conversely, a current containing 125 μ m particles takes almost 30 s and 4 km. The proportion of total travel time spent in turbulent suspension thus decreases with increasing particle size (Fig. 11c) and increases with increasing column height (Fig. 11d–f).

Tall, fine-grained, column collapses transfer their mass slowly to the dense basal flow and are dominated by a dilute turbulent suspension. Volcanic blasts or very energetic fine-grained flows can thus be characterised by dilute current models (Bursik and Woods, 1996; Dade and Huppert, 1996; Neri et al., 2003; Esposti Ongaro et al., 2008). However, short, coarse-grained columns transfer their mass rapidly to the basal flow and transport is dominated by a concentrated suspension flow (e.g. Sparks, 1976; Wilson, 1985) which is able to out-run the original dilute cloud significantly (Druitt et al., 2002a; Calder et al., 2000; Lube et al., 2007a). These currents need to be described by models that incorporate dense granular physics.

Further upper fine ash-cloud surges may be generated from the dense basal flows by shear (Denlinger, 1987), fluidisation (Wilson, 1984) and cold air entrainment (Wilson and Walker, 1982). Thus, fines transferred into the basal flows may be immediately transferred back into further upper fine ash-cloud surges. However, as these are distinct in origin from the original collapsing dilute column, they have

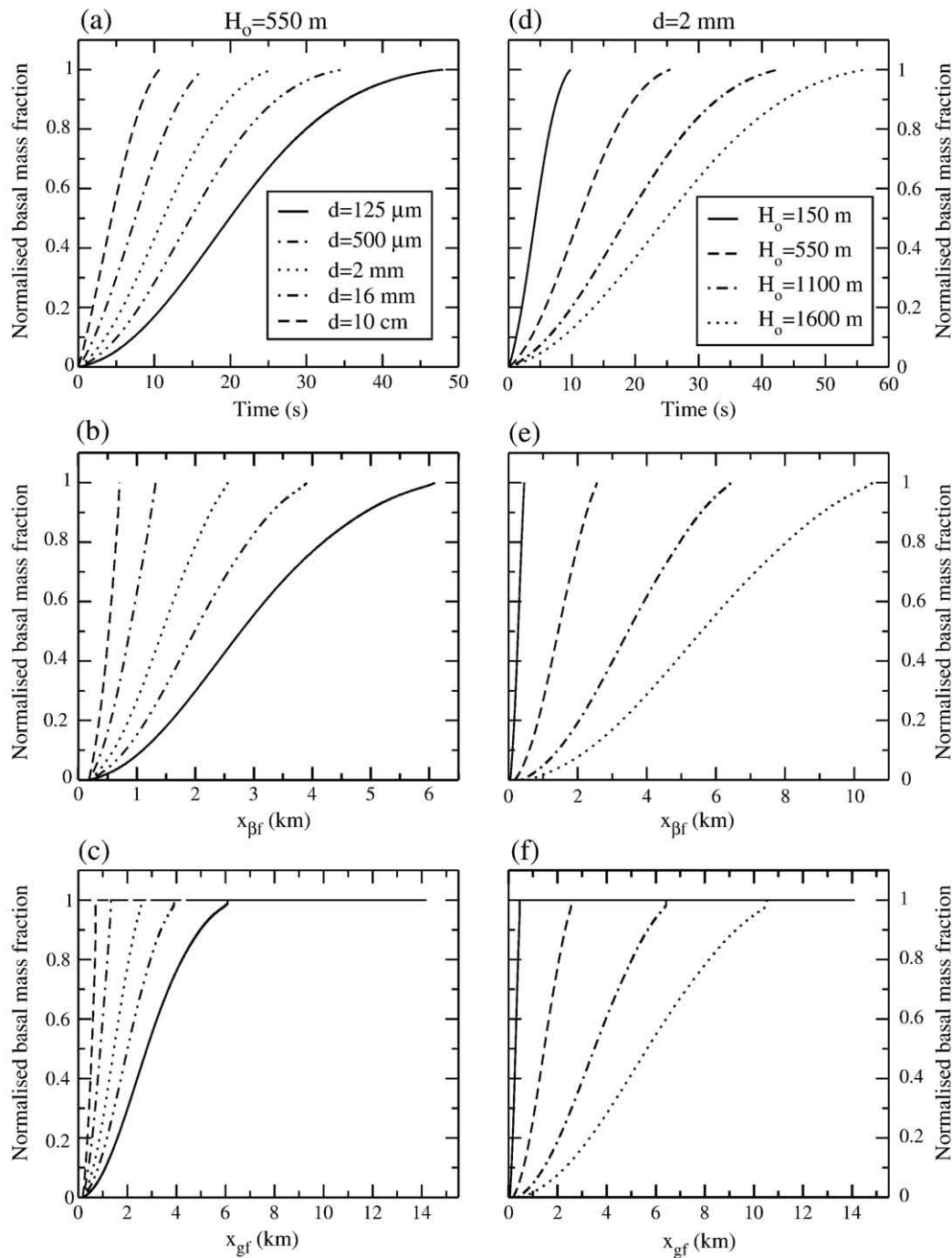


Fig. 11. The ratio of the mass of solids in the dense basal flow M_b , to the total solids mass in the basal flow and the upper dilute current ($M_b + M_a$), normalised by the total mass in the basal flow when the upper dilute current terminates t_{bf} . (a–c) For $H_0 = 550$ m and varied particle size, as indicated. Normalised mass fraction shown (a) with time from column collapse up to t_{bf} , (b) with the upper dilute current front position from the vent x_{bf} , and (c) with dense basal flow front position from the vent x_{gf} . d–f) The same results, but for an initial particle size of 2 mm and varied initial column height, as indicated. For both sets of model calculations $\phi_0 = 0.01$. Lower concentrations result in slower rates of transfer, but have shorter total transfer times due to the lower initial mass of the column. The currents propagate over a 10 km volcanic slope inclined at 13° flanked by a 1° plateau. The dynamic friction angle of the basal flow is $\delta = 10^\circ$.

not been treated in our model. Entrainment of ambient air has been neglected. This, and the elutriation of particles, will dilute the upper current, affecting its sedimentation related runout and the rate the basal layer thickens. This assumption should be relaxed in future development. If a poly-disperse mixture is considered, we expect coarse particles to become concentrated in the basal flow with fine particles in the upper current and significant mass in both layers. These coarse grains are also expected to deposit closer to the source than fine grains. Erosional regimes must also exist (Douady et al.,

1999; Gray, 2001) and could be included when a proper description of the phase transitions between static and flowing states of granular materials becomes available. Future simulations could also investigate the effect of taller eruption columns and sustained eruptions.

This study has implications for the use of pyroclastic flow models in hazards assessment. Single layer models do not include the coupling of the dense and dilute flow regions and thus they may not predict the full behaviour of these complex flows. For example, dense flows may propagate much further than the dilute part of the

current, resulting in an underestimate of the runout distance. The model presented here attempts to address this issue. The future of this field must be to develop coupled models that can take better account of the two-component character of many pyroclastic flows.

Acknowledgments

EED was supported by a UK Natural Environment Research Council PhD grant no: NER/S/A/2003/11201. The research of RSJS is supported by a Royal Society Wolfson Research Merit Award. This work was carried out using the computational facilities of both the Advanced Computing Research Centre and the Department of Mathematics at Bristol University. EED thanks Michael Hudson-Doyle for coding advice, and Gert Lube for helpful discussions. We thank Eliza Calder and an anonymous reviewer for comments that have improved this manuscript.

References

- Bale, D.S., Leveque, R.J., Rossmannith, J.A., 2003. A wave propagation method for conservation laws and balance laws with spatially-varying flux functions. *SIAM J. Sci. Comput.* 24, 955–978.
- Bonnecaze, R.T., Huppert, H.E., Lister, J.R., 1993. Particle-driven gravity currents. *J. Fluid Mech.* 250, 339–369.
- Branney, M.J., Kokelaar, P., 1992. A reappraisal of ignimbrite emplacement: progressive aggradation and changes from particulate to non-particulate flow during emplacement of high-grade ignimbrite. *Bull. Volcanol.* 54, 504–520.
- Branney, M.J., Kokelaar, P., 1997. Giant bed from a sustained catastrophic density current flowing over topography: Acatlán ignimbrite, Mexico. *Geology* 25 (2), 115–118.
- Branney, M.J., Kokelaar, P., 2002. Pyroclastic Density Currents and the Sedimentation of Ignimbrites, Vol. 27 of Memoirs. Geological Society, London, UK.
- Browne, B.L., Gardner, J.E., 2005. Transport and deposition of pyroclastic material from the ~ 1000 a.d. caldera-forming eruption of Volcán Ceboruco, Nayarit, Mexico. *Bull. Volcanol.* 67 (5), 469–489. doi:10.1007/s00445-004-0390-6.
- Bursik, M.I., Woods, A.W., 1991. Buoyant, superbuoyant and collapsing eruption columns. *J. Volcanol. Geotherm. Res.* 45, 347–350.
- Bursik, M.I., Woods, A.W., 1996. The dynamics and thermodynamics of large ash flows. *Bull. Volcanol.* 58, 175–193.
- Calder, E.S., Sparks, R.S.J., Gardeweg, M.C., 2000. Erosion, transport and segregation of pumice and lithic clasts in pyroclastic flows inferred from ignimbrite at lascar volcano, Chile. *J. Volcanol. Geotherm. Res.* 104, 201–235.
- Carazzo, G., Kaminski, E., 2006. The route to self-similarity in turbulent jets and plumes. *J. Fluid Mech.* 547, 137–148.
- Cas, R.A.F., Wright, J.V., 1987. *Volcanic Successions, Modern and Ancient: A Geological Approach to Processes, Products and Successions*. Allen & Unwin Ltd, London, UK.
- Clarke, A.B., Neri, A., Voight, B., Macedonio, G., Druitt, T.H., 2002. Computational modelling of the transient dynamics of the August 1997 Vulcanian explosions at Soufrière Hills Volcano, Montserrat: influence of initial conditions on near-vent pyroclastic dispersal. In: Druitt, T.H., Kokelaar, B.P. (Eds.), *The Eruption of Soufrière Hills Volcano, Montserrat, from 1995 to 1999*, 21. *Geol. Soc. Mem. Geol. Soc. of London*, London, pp. 319–348.
- Cole, P.D., Calder, E.S., Druitt, T.H., Hoblitt, R.P., Robertson, R., Sparks, R.S.J., Young, S.R., 1998. Pyroclastic flows generated by gravitational instability of the 1996–1997 lava dome of Soufrière Hills Volcano, Montserrat (Paper 98GL01510). *Geophys. Res. Lett.* 25 (18), 3425–3428.
- Cole, P.D., Calder, E.S., Sparks, R.S.J., Clarke, A.B., Druitt, T.H., Young, S.R., Herd, R.A., Harford, C.L., Norton, G.E., 2002. Deposits from dome-collapse and fountain-collapse pyroclastic flows at Soufrière Hills Volcano, Montserrat. In: Druitt, T.H., Kokelaar, B.P. (Eds.), *The Eruption of Soufrière Hills Volcano, Montserrat, from 1995 to 1999*, 21. *Geol. Soc. Mem. Geol. Soc. of London*, London, pp. 231–262.
- Dade, W.B., Huppert, H.E., 1996. Emplacement of the Taupo ignimbrite by a dilute turbulent flow. *Nature* 381, 509–512.
- Darteville, S., Rose, W.I., Stix, J., Kelfoun, K., Vallance, J.W., 2004. Numerical modeling of geophysical granular flows: 2. Computer simulations of Plinian clouds and pyroclastic flows and surges. *G-cubed* 5 (8), Q08004. doi:10.1029/2003GC000637.
- Denlinger, R.P., 1987. A model for generation of ash clouds by pyroclastic flows, with application to the 1980 eruptions at Mount St. Helens, Washington. *J. Geophys. Res.* 92 (B10), 10,284–10,298.
- Denlinger, R.P., Iverson, R.M., 2001. Flow of variably fluidised granular masses across three-dimensional terrain: 2. Numerical predictions and tests. *J. Geophys. Res.* 106, 553–566.
- Denlinger, R.P., Iverson, R.M., 2004. Granular avalanches across irregular three-dimensional terrain: 1. Theory and computation. *J. Geophys. Res.* 109, F01014. doi:10.1029/2003JF000085.
- Dobran, F., Neri, A., Macedonio, G., 1993. Numerical simulations of collapsing volcanic columns. *J. Geophys. Res.* 98 (B3), 4231–4259.
- Douady, S., Androetti, B., Daerr, A., 1999. On granular surface flow equations. *Eur. Phys. J. B* 11, 131–142.
- Doyle, E.E., 2008. Analogue and numerical modelling of gravity currents and pyroclastic flows. Ph.D. thesis, Department of Earth Sciences, University of Bristol, UK.
- Doyle, E.E., Hogg, A.J., Mader, H.M., Sparks, R.S.J., 2008. Modeling dense pyroclastic basal flows from collapsing columns. *Geophys. Res. Lett.* 35, L04305. doi:10.1029/2007GL032585.
- Doyle, E.E., Huppert, H.E., Lube, G., Mader, H.M., Sparks, R.S.J., 2007. Static and flowing regions in granular collapses down channels: insights from a sedimenting shallow water model. *Phys. Fluids* 19 (10), 106601. doi:10.1063/1.2773738.
- Druitt, T.H., 1992. Emplacement of the 18 May 1980 lateral blast deposit ENE of Mount St. Helens, Washington. *Bull. Volcanol.* 54, 554–572.
- Druitt, T.H., 1998. Pyroclastic density currents. In: Gilbert, J., Sparks, R. (Eds.), *The Physics of Explosive Volcanic Eruptions*. Geological Society, London, Special Publications, 145. Geological Society, London, pp. 145–182.
- Druitt, T.H., Calder, E.S., Cole, P.D., Hoblitt, R.P., Loughlin, S.C., Norton, G.E., Ritchie, L.J., Sparks, R.S.J., Voight, B., 2002a. Small-volume, highly mobile pyroclastic flows formed by rapid sedimentation from pyroclastic surges at Soufrière Hills Volcano, Montserrat: an important volcanic hazard. In: Druitt, T.H., Kokelaar, B.P. (Eds.), *The Eruption of Soufrière Hills Volcano, Montserrat, from 1995 to 1999*, 21. *Geol. Soc. Mem. Geol. Soc. of London*, London, pp. 263–279.
- Druitt, T.H., Sparks, R.S.J., 1982. A proximal ignimbrite breccia facies on Santorini, Greece. *J. Volcanol. Geotherm. Res.* 13, 147–171.
- Druitt, T.H., Young, S.R., Baptie, B., Bonadonna, C., Calder, E.S., Clarke, A.B., Cole, P.D., Harford, C.L., Herd, E.A., Luckett, R., Ryan, G., Voight, B., 2002b. Episodes of cyclic Vulcanian explosive activity with fountain collapse at Soufrière Hills Volcano, Montserrat. In: Druitt, T.H., Kokelaar, B.P. (Eds.), *The Eruption of Soufrière Hills Volcano, Montserrat, from 1995 to 1999*, 21. *Geol. Soc. Mem. Geol. Soc. of London*, London, pp. 281–306.
- Dufek, J., Bergantz, M., 2007. The suspended-load and bed-load transport of particle laden gravity currents: insight from pyroclastic flows that traverse water. *Theor. Comput. Fluid Dynam.* 21, 119–145.
- Dufek, J., Manga, M., 2008. In situ production of ash in pyroclastic flows. *J. Geophys. Res.* 113, B09207. doi:10.1029/2007JB005555.
- Esposito Ongaro, T., Clarke, A.B., Neri, A., Voight, B., Widiwidijanti, C., 2008. Fluid dynamics of the 1997 Boxing Day volcanic blast on Montserrat, W.I. *J. Geophys. Res.* B03211. doi:10.1029/2006JB004898.
- Fisher, R.V., 1979. Models for pyroclastic surges and pyroclastic flows. *J. Volcanol. Geotherm. Res.* 6, 305–318.
- Fisher, R.V., 1990. Transport and deposition of a pyroclastic surge across an area of high relief: the 18 May 1980 eruption of Mount St. Helens, Washington. *Geol. Soc. Am. Bull.* 102, 1038–1054.
- Fisher, R.V., 1995. Decoupling of pyroclastic currents: hazards assessments. *J. Volcanol. Geotherm. Res.* 66, 257–263.
- Fisher, R.V., Schmincke, H.-U., 1984. *Pyroclastic Rocks*. Springer-Verlag, Berlin, Heidelberg, New York, Tokyo.
- Freundt, A., 1999. Formation of high grade ignimbrites Part II. A pyroclastic suspension current model with implications also for low-grade ignimbrites. *Bull. Volcanol.* 60, 545–567.
- Freundt, A., Schmincke, H.-U., 1985. Lithic-enriched segregation bodies in pyroclastic flow deposits of Laacher See volcano (East Eifel, Germany). *J. Volcanol. Geotherm. Res.* 25, 193–224.
- Giordano, G., Dobran, F., 1994. Computer simulations of the Tuscalano Artemisio's second pyroclastic flow unit (Alban Hills, Latium, Italy). *J. Volcanol. Geotherm. Res.* 61, 69–94.
- Gray, J.M.N.T., 2001. Granular flow in partially filled slowly rotating drums. *J. Fluid Mech.* 441, 1–29.
- Gray, J.M.N.T., Wieland, M., Hutter, K., 1999. Gravity-driven free surface flow of granular avalanches over complex basal topography. *Proc. Roy. Soc. London A: Mathemat. Phys. Engin. Sci.* 455, 1841–1874.
- Hoblitt, R.P., 1986. Observations of eruptions, July 22 and August 7, 1980, at Mount St. Helens, Washington. *U.S.G.S. Prof. Pap.* 1335, 1–43.
- Hogg, A.J., Pritchard, D., 2004. The effects of hydraulic resistance on dam-break and other shallow inertial flows. *J. Fluid Mech.* 501, 179–212.
- Hubbard, M.E., Garcia-Navarro, P., 2000. Flux difference splitting and the balancing of source terms and flux gradients. *J. Comput. Phys.* 165, 89–125.
- Hughes, S.R., Druitt, T.H., 1998. Particle fabric in a small, type-2 ignimbrite flow unit (Laacher See, Germany) and implications for emplacement dynamics. *Bull. Volcanol.* 60, 125–136.
- Iverson, R.M., Denlinger, R.P., 2001. Flow of variably fluidized granular masses across three-dimensional terrain. 1. Coulomb mixture theory. *J. Geophys. Res.* 106, 537–552.
- Kaminski, E., Jaupart, C., 1998. The size distribution of pyroclasts and the fragmentation sequence in explosive volcanic eruptions. *J. Geophys. Res. - Solid Earth* 103 (B12), 29759–29779.
- Kelfoun, K., Samaniego, P., Palacios, P., Barba, D., 2009. Testing the suitability of frictional behaviour for pyroclastic flow simulation by comparison with a well-constrained eruption at tungurahua volcano (Ecuador). *Bull. Volcanol.* 71 (9), 1057–1075. doi:10.1007/s00445-009-0286-6.
- Lacroix, A., 1904. *La Montagne Pelée et ses éruptions*. Masson et Cie, Paris, in French.
- Leveque, R.J., 2002. Finite volume methods for hyperbolic problems. *Cambridge Texts in Applied Mathematics*. Cambridge University Press, Cambridge, UK.
- Levine, A., Kieffer, S., 1991. Hydraulics of the August 7, 1980, pyroclastic flow at Mount St. Helens, Washington. *Geology* 19, 1121–1124.
- Lube, G., Cronin, S., Platz, T., Freundt, A., Procter, J.N., Henderson, C., Sheridan, M.F., 2007a. Flow and deposition of pyroclastic granular flows: a type example from the 1975 Ngauruhoe eruption, New Zealand. *J. Volcanol. Geotherm. Res.* 161 (4), 362–363.
- Lube, G., Huppert, H.E., Sparks, R.S.J., Freundt, A., 2007b. Static and flowing regions in granular collapses down channels. *Phys. Fluids* 19 (4), 043301. doi:10.1063/1.2712431.
- Mangeney, A., Heinrich, P., Roche, R., 2000. Analytical solution for testing debris avalanche and numerical models. *Pure and Appl. Geophys.* 157, 1081–1096.

- Mangeny-Castelnaud, A., Vilotte, J.P., Bristeau, M.O., Perthame, B., Bouchut, F., Simeoni, C., Yermeni, S., 2003. Numerical modeling of avalanches based on Saint Venant equations using a kinetic scheme. *J. Geophys. Res.* 108 (B11), 2527–2545.
- Martin, D., Nokes, R., 1989. A fluid-dynamical study of crystal settling in convecting magmas. *J. Petrol.* 30 (6), 1471–1500.
- Mellors, R.A., Waitt, R.B., Swanson, D.A., 1988. Generation of pyroclastic flows and surges by hot-rock avalanches from the dome of Mount St. Helens volcano, USA. *Bull. Volcanol.* 50, 14–25.
- Nairn, I.A., Self, S., 1978. Explosive eruptions and pyroclastic avalanches from Ngauruhoe in February 1975. *J. Volcanol. Geotherm. Res.* 3, 39–60.
- Neri, A., Dobran, F., 1994. Influence of eruption parameters on the thermofluid dynamics of collapsing volcanic columns. *J. Geophys. Res.* 99 (B6), 11833–11857.
- Neri, A., Esposti Ongaro, T.E., Macedonio, G., Gidaspow, D., 2003. Multiparticle simulation of collapsing volcanic columns and pyroclastic flow. *J. Geophys. Res.* 108 (B4), 2202–2224.
- Neri, A., Macedonio, G., 1996. Numerical simulation of collapsing volcanic columns with particles of two sizes. *J. Geophys. Res.* 101 (B4), 8153–8174.
- Palladino, D.M., Valentine, G.A., 1995. Coarse-tail vertical and lateral grading in pyroclastic flow deposits of the Latera Volcanic Complex (Vulsini, central Italy): origin and implications for flow dynamics. *J. Volcanol. Geotherm. Res.* 69, 343–364.
- Patra, A.K., Bauer, A.C., Nichita, C.C., Pitman, E.B., Sheridan, M.F., Bursik, M., Rupp, B., Webber, A., Stinton, A., Namikawa, L.M., Renschler, C.S., 2005. Parallel adaptive numerical simulation of dry avalanches over natural terrain. *J. Volcanol. Geotherm. Res.* 139, 1–21.
- Pitman, E., Patra, A., Bauer, A., Sheridan, M., Bursik, M., 2003. Computing debris flows and landslides. *Phys. Fluids* 15 (12), 3638–3646.
- Pouliquen, O., 1999. Scaling laws in granular flows down rough inclined planes. *Phys. Fluids* 11 (3), 542–548.
- Pouliquen, O., Forterre, Y., 2002. Friction law for dense granular flows: application to the motion of a mass down a rough inclined plane. *J. Fluid Mech.* 453, 133–151.
- Pudasaini, S.P., Hutter, K., 2007. *Avalanche dynamics. Dynamics of rapid flows of dense granular flows.* Springer, Berlin, Heidelberg, New York.
- Roche, O., Gilbertson, M.A., Phillips, J.C., Sparks, R.S.J., 2002. Experiments on deaerating granular flows and implications for pyroclastic flow mobility. *Geophys. Res. Lett.* 29 (16).
- Roche, O., Gilbertson, M.A., Phillips, J.C., Sparks, R.S.J., 2004. Experimental study of gas-fluidized granular flows with implications for pyroclastic flow emplacement. *J. Geophys. Res. - Solid Earth* 109 (B10), B10201.
- Rowley, P.D., Kuntz, M.A., Macleod, N.S., 1981. The 1980 eruptions of Mount St Helens, Washington: pyroclastic-flow deposits. In: Lipman, P.W., Mullineaux, D.R. (Eds.), *The Eruption of Soufriere Hills Volcano, Montserrat, from 1995 to 1999*, 1250. *Geol. Surv. Prof. Pap. USGS*, London, pp. 489–512.
- Savage, S.B., Hutter, K., 1989. The motion of a finite mass of granular material down a rough incline. *J. Fluid Mech.* 199, 177–215.
- Smith, R.L., 1960a. Ash flows. *Geol. Soc. Amer. Bull.* 71, 795–842.
- Smith, R.L., 1960b. Zones and zonal variations in welded ash flows. *U.S.G.S. Prof. Paper* 354-F, pp. 149–159.
- Sparks, R., Bursik, M., Carey, S., Gilbert, J., Glaze, L., Sigurdsson, H., Woods, A., 1997. *Volcanic Plumes.* Wiley, New Jersey.
- Sparks, R.S.J., 1976. Grain size variations in ignimbrites and implications for the transport of pyroclastic flows. *Sedimentology* 23, 147–188.
- Sparks, R.S.J., Barclay, J., Calder, E.S., Herd, R.A., Komorowski, J.-C., Lockett, R., Norton, G. E., Ritchie, L.T., Voight, B., Woods, A.W., 2002. Generation of a debris avalanche and violent pyroclastic density current on 26 December (Boxing day) 1997 at Soufrière Hills Volcano, Montserrat. In: Druitt, T.H., Kokelaar, B.P. (Eds.), *The Eruption of Soufriere Hills Volcano, Montserrat, from 1995 to 1999*, 21. *Geol. Soc. Mem. Geol. Soc. of London*, London, pp. 409–434.
- Sparks, R.S.J., Self, S., Walker, G.P.L., 1973. Products of ignimbrite eruptions. *Geology* 1 (3), 115–118.
- Sparks, R.S.J., Wilson, L., 1976. A model for the formation of ignimbrite by gravitational column collapse. *J. Geol. Soc. Lond.* 132, 441–451.
- Sparks, R.S.J., Wilson, L., Hulme, G., 1978. Theoretical modeling of the generation, movement and emplacement of pyroclastic flows by column collapse. *J. Geophys. Res.* 83 (B4), 1727–1739.
- Takahashi, T., Tsujimoto, H., 2000. A mechanical model for Merapi-type pyroclastic flow. *J. Volcanol. Geotherm. Res.* 98, 91–115.
- Timmermans, M.E., Lister, J.R., Huppert, H.E., 2001. Compressible particle-driven gravity currents. *J. Fluid Mech.* 445, 305–325.
- Turner, J.S., 1966. Jets and plumes with negative or reversing buoyancy. *J. Fluid Mech.* 26, 779–792.
- Valentine, G.A., 1987. Stratified flow in pyroclastic surges. *Bull. Volcanol.* 49, 616–630.
- Valentine, G.A., Fisher, R., 1986. Origin of layer 1 deposits in ignimbrites. *Geology* 14 (2), 146–148.
- Wadge, G., Jackson, P., Bower, S.M., Woods, A.W., Calder, E., 1998. Computer simulations of pyroclastic flows from dome collapse. *Geophys. Res. Lett.* 25 (19), 3677–3680.
- Walker, G.P.L., 1971. Grain size characteristics of pyroclastic deposits. *J. Geol.* 79, 696–714.
- Walker, G.P.L., Wilson, C.J.N., 1983. Lateral variations in the Taupo ignimbrite. *J. Volcanol. Geotherm. Res.* 18, 117–133.
- Widiwijayanti, C., Voight, B., Hidayat, D., Schilling, S.P., 2009. Objective rapid delineation of areas at risk from block-and-ash pyroclastic flows and surges. *Bull. Volcanol.* 71 (6), 687–703. doi:10.1007/s00445-008-0254-6.
- Wilson, C.J.N., 1984. The role of fluidization in the emplacement of pyroclastic flows, 2: Experimental results and their interpretation. *J. Volcanol. Geotherm. Res.* 20, 55–84.
- Wilson, C.J.N., 1985. The Taupo eruption, New Zealand II. the Taupo ignimbrite. *Phil. Trans. Royal Soc. Lond. Ser. A. Math. Phys. Sci.* 314, 229–310.
- Wilson, C.J.N., 1986. Pyroclastic flows and ignimbrites. *Sci. Prog. Oxf.* 70, 171–207.
- Wilson, C.J.N., Walker, G.P.L., 1982. Ignimbrite depositional facies: the anatomy of a pyroclastic flow. *J. Geol. Soc. Lond.* 139, 581–592.
- Wilson, L., Sparks, R.S.J., Walker, G.P.L., 1980. Explosive volcanic eruptions—IV. The control of magma properties and conduit geometry on eruption column behaviour. *Geophys. J. R. Astron. Soc.* 63, 117–148.
- Woods, A.W., Bursik, M.L., 1991. Particle fallout thermal disequilibrium and volcanic plumes. *Bull. Volcanol.* 53, 559–570.
- Wright, J.V., Walker, G.P., 1981. Eruption, transport and deposition of ignimbrite: a case study from Mexico. *J. Volcanol. Geotherm. Res.* 9, 111–131.